Chinese Chemical Letters 33 (2022) 4428–4436

Contents lists available at ScienceDirect

Chinese Chemical Letters

journal homepage: www.elsevier.com/locate/cclet

# Recent progress on preparation and applications of layered double hydroxides

Mengting Duan[a], Shanjing Liu[a], Qiming Jiang[a], Xingmei Guo[a,*], Junhao Zhang[a,*], Shenglin Xiong[b,*]

[a] School of Environmental and Chemical Engineering, Jiangsu University of Science and Technology, Zhenjiang 212003, China
[b] Key Laboratory of Colloid and Interface Chemistry, Ministry of Education, and School of Chemistry and Chemical Engineering, Shandong University, Ji'nan 250100, China

ARTICLE INFO

*Article history:*
Received 5 November 2021
Revised 3 December 2021
Accepted 15 December 2021
Available online 20 December 2021

*Keywords:*
Layered double hydroxides
Anion exchangeability
Structural adjustability
Performance tunability

ABSTRACT

The properties of layered double hydroxides (LDHs), including the adjustability of cations in host layers, exchangeability of anions between layers, and tunability of the crystal structure, render them unique characteristics in preparation and applications. Relating to the structural characteristics of LDHs, this work analyzes the research status, advantages and disadvantages of the synthetic methods for LDHs, including hydrothermal, electrodeposition, co-precipitation and anion exchange methods. In addition, the application status and prospects are reviewed, such as photo/electrocatalysis, electrochemical energy storage, magnetic materials, pollutant adsorption, and other fields. Lastly, the critical issues and solutions in the developing process of LDHs are analyzed and proposed.



## 1. Introduction

Layered double hydroxides (LDHs) are expressed by a general formula of $[M^{2+}_{1-x}\ M^{3+}_{x}\ (OH)_2]^{2+}\ [A^{n-}_{x/n} \cdot\ m\ H_2O]$ [1,2], where $M^{2+}$ and $M^{3+}$ represent the positively charged divalent and trivalent metal cations, respectively. For example, $Fe^{3+}$ [3], $Fe^{2+}$, $Al^{3+}$ [4], $Mn^{2+}$[5,6], $Zn^{2+}$ [7], $Co^{2+}$ [8,9], $Mg^{2+}$[10], $Ni^{2+}$ [11,12], $Cu^{2+}$ [13], $Cr^{2+}$ [14] have been frequently studied. $A^{n-}$ represents negatively charged anions, which can balance the charge and keep the LDHs electrically neutral as a whole [15]. As shown in Fig. 1, LDHs have a sandwich-like structure [16]. The host layers of hydroxide are constructed by regular octahedral units composed of $M^{2+}$, $M^{3+}$ and hydroxide ions. The metal cation occupies the central position of the octahedron formed by hydroxide ions. Under the action of van der Waals force and covalent bonds, the octahedrons are arranged regularly into a two-dimensional (2D) structure, and the host layers are positively charged as a whole. The adjacent host layers are filled with $A^{n-}$ and water molecules, called the guest layers [17,18]. The host layers and the guest layers with different charges are stacked alternately through electrostatic interaction, hydrogen bonding and van der Waals force, *etc.* When the molar ratio "x" of trivalent metal cations to all metal cations is in the range of 0.2 to 0.33, the radius of $M^{2+}$ and $M^{3+}$ are close, and it is easier to obtain LDHs with a single crystal phase.

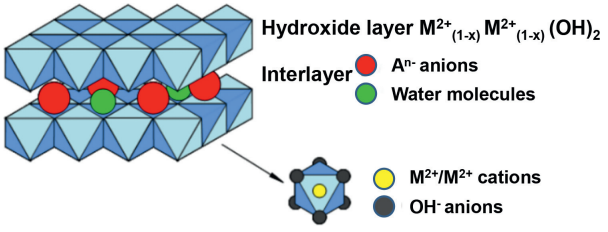


**Fig. 1.** Schematic diagram of the structure of LDHs. Reproduced with permission [16]. Copyright 2019, American Chemical Society.

It is worth noting that certain ions can overcome the interaction between the layers of LDHs, and reversibly insert into the interlaminar interstitial spaces without destroying the host layer structure. The local electronic coupling between the newly inserted ions and the cations in the layers can change the electronic structure of the host layers, providing a new pathway for the optimization and modification of intercalation materials [19]. In addition, the LDHs have also been exfoliated to form a single layer structure and the new type of nanosheet with 2D anisotropy exhibits significantly different performance from the stacked structure [20].

* Corresponding authors.
*E-mail addresses:* guoxm@just.edu.cn (X. Guo), jhzhang6@just.edu.cn (J. Zhang), chexsl@sdu.edu.cn (S. Xiong).

https://doi.org/10.1016/j.cclet.2021.12.033
1001-8417/

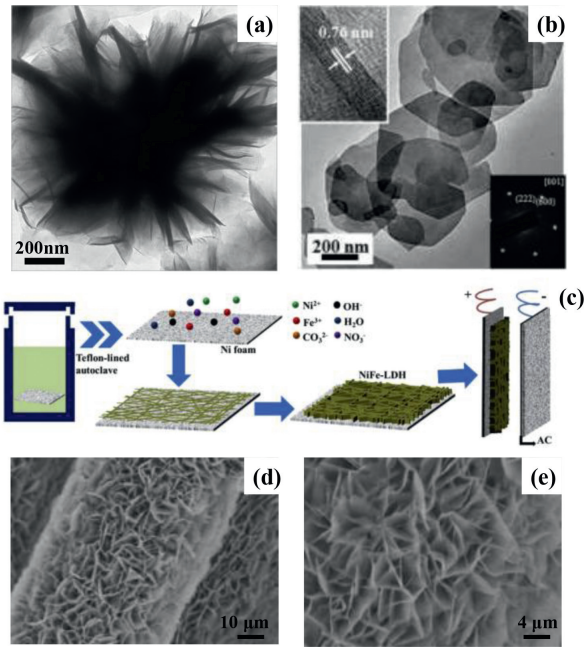


**Fig. 2.** (a) TEM image of AlNi LDH. Reproduced with permission [27]. Copyright 2017, Elsevier. (b) TEM image and selected area electron diffraction (SAED) result of $NiCo_2Al$ LDH. Reproduced with permission [28]. Copyright 2017, Elsevier. (c) The formation mechanism and application scheme of NiFe LDH films supported on nickel foams. Reproduced with permission [29]. Copyright 2017, Elsevier. (d, e) SEM images of NiCo LDH. Reproduced with permission [30]. Copyright 2019, Elsevier.

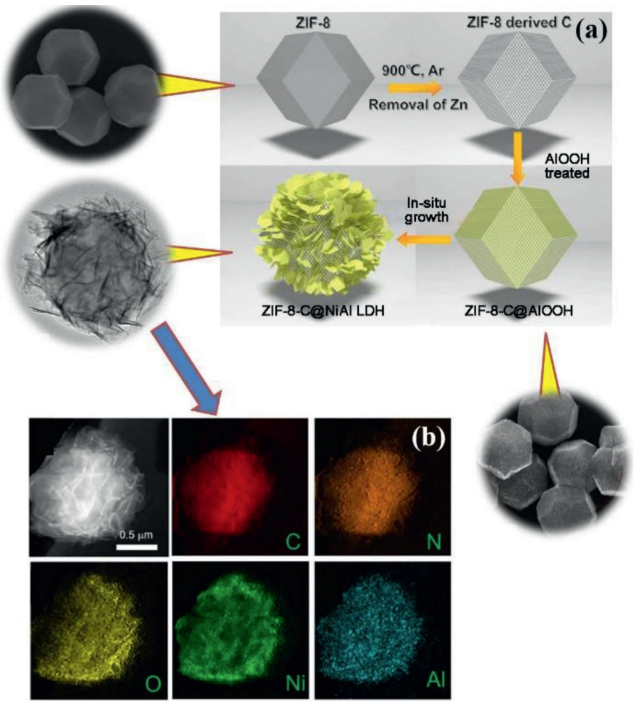


**Fig. 3.** (a) Schematic illustration for the fabrication of ZIF-8-C@NiAl LDH core/shell hierarchical polyhedrons. (b) STEM image of ZIF-8-C@NiAl LDH nanocomposite and corresponding elemental mappings. Reproduced with permission [33]. Copyright 2018, Elsevier.

## 2. Preparation methods of LDHs

### 2.1. Hydrothermal method

Hydrothermal method, also known as the one-pot method, was firstly used by geologists to simulate the mineralization principle in nature, and then gradually applied to the study of functional materials, which is a common method for preparing crystals. For LDHs preparation, salt solutions containing $M^{2+}$ and $M^{3+}$ are mixed and placed in a closed pressure vessel, where the critical or supercritical reaction occurs under high temperature and high pressure conditions, followed by centrifugation, washing, and drying to obtain the final product [21–23]. In the hydrothermal process, reagents with the function of slow hydrolysis, such as urea, are often added to promote the material to crystallize in the 2D direction and form a stable ultra-thin structure. Cations in the host layers are controllable by changing the cation species and the molar ratio of $M^{2+}$ and $M^{3+}$. Currently, researchers have developed LDHs ranging from unitary to ternary [24,25]. Song and co-workers [26] reported the synthesis of CoCo, NiCo and NiFe LDHs materials *via* a topochemical approach. Among them, the CoCo LDHs material is a typical unitary LDHs. Zhang's group [27] took advantage of the hydrolysis and coordination of urea to synthesize AlNi LDH by hydrothermal method. The transmission electron micrograph (TEM) of the AlNi LDH is shown in Fig. 2a, the edge folds morphology of the flower-like structure proves that the prepared AlNi LDH is composed of ultra-thin nanosheet. Xiao *et al.* [28] prepared ternary $NiCo_2Al$ LDHs with hexagonal nanosheet structure under hydrothermal conditions shown in Fig. 2b.

In addition, by adding matrix material to the precursor solution, LDHs will preferentially nucleate and grow on the matrix. For example, Fang *et al.* [29] utilized hydrothermal method to vertically grow NiFe LDH nanosheets on the surface of three-dimensional (3D) macroporous nickel foam (NF). The formation process and mechanism are shown in Fig. 2c. $OH^-$ produced by hydrolysis of urea firstly reacts with $Ni^{2+}$ and $Fe^{3+}$ to generate nickel and iron hydroxide monomers, which gather on the surface of NF. As the hydrothermal time increases, more $OH^-$ is released into the solution. $Ni(OH)_2$ and $Fe(OH)_3$ microcrystals continue to aggregate and interact, begin to grow along the vertical direction of NF, and gradually form NiFe LDH nanosheets. In this process, charge transfer occurs between $Ni^{2+}$ and $Fe^{3+}$, which leads to redistribution of the electron densities [30,31]. In addition, hexamethylenetetramine (HMT) is also used as a hydrolysis agent for hydrothermal synthesis of LDHs. For example, Jiang and co-workers [32] used carbon fiber (CF) as substrate, $Ni(NO_3)_2{\cdot}6H_2O$, $Co(NO_3)_2{\cdot}6H_2O$ and HMT as precursor solutions, to synthesize NiCo LDH grown on CF under hydrothermal conditions. From the SEM images in Figs. 2c and d, it can be seen that NiCo LDH nanosheets grow vertically and uniformly on the CF to form stable LDH nanosheets arrays.

With the deepening of research and expansion of ideas, people began to seek new substrates or templates to obtain LDHs with various morphologies. For example, Han's group [33] firstly annealed the 3D metal organic framework of zeolitic imidazolate framework-8 (ZIF-8) to obtain ZIF-8 derived porous carbon material (ZIF-8-C). Then, ZIF-8-C was used as template and immersed in a AlOOH precusor solution to obtain a core-shell structure of ZIF-8-C/AlOOH. After that, ZIF-8-C/AlOOH was dispersed in an aqueous solution containing $Ni(NO_3)_2{\cdot}6H_2O$ and urea. Under hydrothermal conditions, NiAl LDH was crystallized in situ on the ZIF-8-C polyhedron to form a 3D nanoporous carbon/NiAl LDH core-shell nanocomposite (ZIF-8-C@NiAl LDH). Fig. 3a shows the shapes of the ZIF-8-C@NiAl LDH core-shell hierarchical polyhedron, the ZIF-8-C polyhedron, ZIF-8-C/AlOOH polyhedron and ZIF-8-C formed during the synthesis process appearance. The SEM and TEM images of the ZIF-8-C@NiAl LDH core-shell structure clearly show that the LDH lamellae are grown vertically and intersectingly on the ZIF-8-C polyhedron, forming a 3D multi-level core-shell structure. Fig. 3b is the scanning transmission electron micrograph (STEM) of the ZIF-8-C@NiAl-LDH nanocomposite material and the corre-

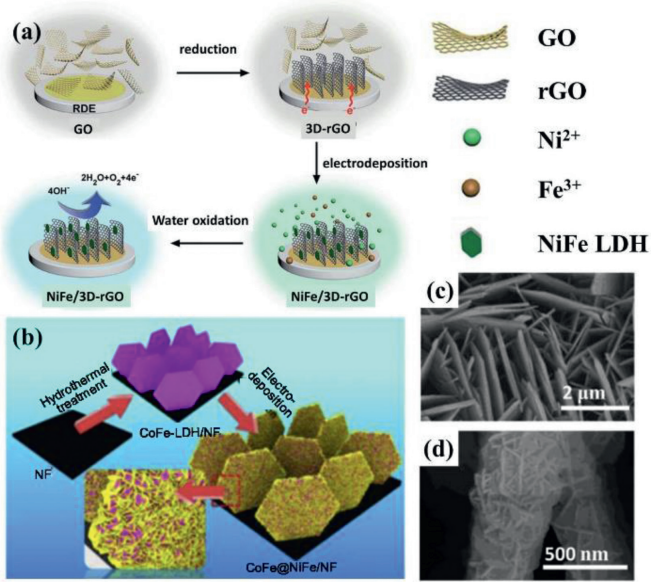


**Fig. 4.** (a) Fabrication and application of the NiFe/3D-rGO electrode using electrodeposition. Reproduced with permission [38]. Copyright 2015, Royal Society of Chemistry. (b) Schematic diagram for the fabrication of CoFe@NiFe/NF architecture using hydrothermal-electrodeposition method. (c, d) SEM images of CoFe LDH/NF and CoFe@ NiFe/NF structure. Reproduced with permission [39]. Copyright 2019, Elsevier.

sponding element mapping. It can be seen that C, N, O, Ni and Al are evenly distributed throughout the core-shell structure, indicating that NiAl LDH has successfully grown on the carbon polyhedron.

In short, hydrothermal method is a widely used technique for preparing LDHs. Under template or template-free conditions, $OH^-$ ions released by the hydrolysis of urea and HMT react with metal ions to form hydroxide core. As the hydrolysis time increases, more $OH^-$ is released into the solution, and different hydroxides continue to aggregate and interact to form LDHs nanosheets [33,34]. Changing the species and concentration of the metal salt solution can control the interlayer cations and structure. Obviously, hydrothermal method can effectively prepare LDHs with uniformity, high purity and good crystallinity. The disadvantage is that the one-pot reaction makes the nucleation and growth process of LDHs lack of precise control and mature theoretical guidance.

### 2.2. Electrodeposition method

Electrodeposition method is also called electrochemical method. It usually takes nitrate, sulfate, hypophosphite and other solutions that can provide suitable metal ions and anions as electrolyte, and uses a three-electrode system to perform cathodic electrodeposition under constant current or potential conditions. $OH^-$ produced by reducing nitrate, sulfate and hypophosphite causes local pH changes of electrolytes (*e.g.*, $NO_3^{2-} + 6H_2O + 8e^- = NH_3 + 9OH^-$), thereby promoting the formation of LDHs on the working electrode ($M^{n+} + nOH^- = M(OH)_n$ [35–37].

For instance, Shi *et al.* [38] used 3D reduced graphene oxide (3D-rGO) obtained by electrochemical reduction as the working electrode, Pt sheet and saturated calomel electrode as the counter and reference electrode, respectively. A mixed solution of $Ni(NO_3)_2{\cdot}6H_2O$ and $Fe(NO_3)_3{\cdot}9H_2O$ was used as electrolyte. Electrodeposition was carried out at different potentials from −0.8 V to −1.3 V, and it only takes 10 s to grow a large amount of NiFe LDH on 3D-rGO. As shown in Fig. 4a, the obtained composite can be further used for electrocatalytic oxidation of water. Besides, electrodeposition can be combined with hydrothermal to obtain hybrid LDHs. For example, Li *et al.* [39] firstly synthesized CoFe LDH by hydrothermal method on NF, and then use CoFe LDH/NF as working electrode to further grow NiFe LDH *via* electrodeposition. During electrodeposition, a mixed solution of $Ni(NO_3)_2{\cdot}6H_2O$ and $FeSO_4{\cdot}7H_2O$ was used as electrolyte, and a constant potential of −1.0 V was applied and maintained for 50 s, 100 s, 200 s, and 300 s, respectively. The synthesis diagram is shown in Fig. 4b. The as obtained NiFe LDH grown on CoFe LDH/NF was named CoFe@NiFe/NF. The SEM image of the hydrothermally synthesized CoFe LDH/NF in Fig. 4c shows that CoFe LDH grows vertically on NF. The SEM image of NiFe LDH electrodeposited on CoFe LDH/NF for 200 s shows that NiFe LDH grows in the vertical direction on the substrate, as shown in Fig. 4d. This work combines the hydrothermal method with the electrodeposition method, and the prepared CoFe@NiFe/NF material has a hierarchical structure of nanosheets on nanosheets, which can provide a larger specific surface area and more active sites.

Electrodeposition is a fast, simple and environmentally friendly method for the synthesis of LDHs. The thickness and performances of the as-obtained LDHs films can be modulated by controlling the concentration of the metal salt solution and the deposition time. During the electrodeposition process, it is not necessary to adjust the pH value of the solution with alkaline substances to avoid the inadvertent formation of hydroxide particles in the solution and obtain purer LDHs [40]. In addition, it can be directly synthesized on various conductive substrates, such as glassy carbon electrodes, titanium plates, copper plates, NF or stainless steel at room temperature without adding adhesives [41]. As an important in-situ deposition method, the substrates can greatly inhibit the aggregation of LDHs nanosheets, and the high mechanical strength of the substrates can buffer the volume change in the subsequent process, avoiding structural collapse and loss of active materials [22]. This method is expected to be used in the development and preparation of high-performance electrodes.

### 2.3. Co-precipitation method

Co-precipitation is conducted by mixing two or more metal salt solutions, and adding NaOH and $Na_2CO_3$ to adjust the pH value of the solution. Under the action of the precipitant NaOH, different metals in the solution crystallize and precipitate simultaneously to obtain target LDHs [42–44].

Huang and co-workers [45] prepared $Ni_xFe$ LDHs ($Ni_2Fe$ LDHs, $Ni_3Fe$ LDHs, $Ni_4Fe$ LDHs and $Ni_5Fe$ LDHs) by co-precipitation method. Cations and the structure of LDHs laminates were controlled by adjusting the molar ratio of nickel nitrate and iron nitrate. The smaller the ratio of $Ni^{2+}$:$Fe^{3+}$, the more beneficial for the formation of $Fe(OH)_3$; the greater the ratio, the more beneficial for the formation of $Ni(OH)_2$. When the molar ratio of $Ni^{2+}$ and $Fe^{3+}$ is 3:1, it is easiest to get a regular lamellar stacks structure. The reason is that under this ratio, the regular octahedral units of the host layers have the highest matching degree, and it is not easy to collapse. This work controls the morphology of LDHs by adjusting the concentration of cations. In addition, Müller's group [46] and Li's group [47] also realized controllable adjustment of LDHs layer spacings by adjusting the types of host cations and guest anions.

Due to the low conductivity of LDHs, when applied to electrode materials, functional components with high conductivity are usually inserted between LDHs layers to improve their performance. In addition to improving the electron transmission efficiency of the material, this method can also adjust the electrochemical performances, thanks to the interface effect and electronic coupling between the functional components and the LDHs layers. For example, Chen's group [48] used a low-temperature co-

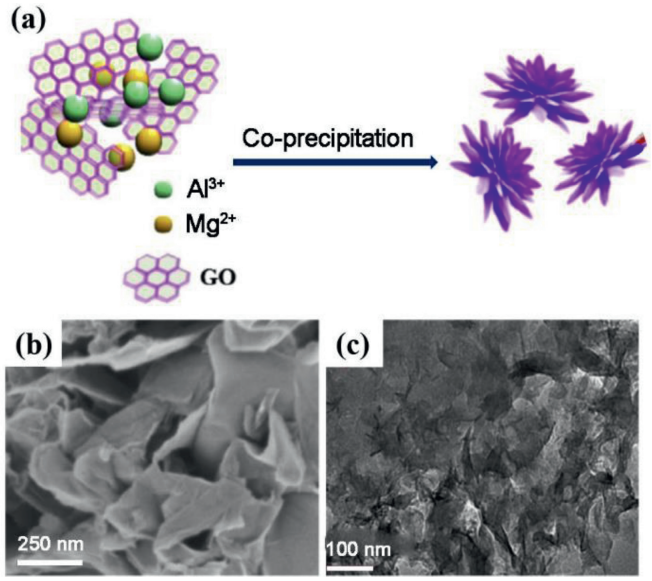


**Fig. 5.** (a) Schematic illustration for the fabrication process of MgAl LDH-GO. (b, c) SEM and TEM images of MgAl LDH-GO. Reproduced with permission [49]. Copyright 2020, Elsevier.

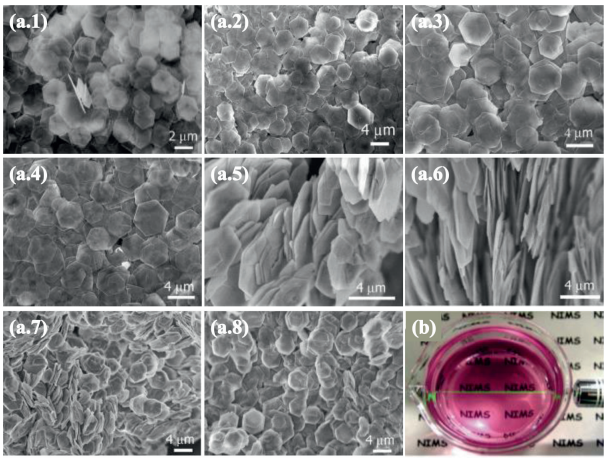


**Fig. 6.** The SEM images of (a.1) CoAl $CO_3^{2-}$ LDHs, (a.2) CoAl $Cl^-$ LDHs, (a.3) CoAl $Cl^-$ LDHs, (a.4) CoAl $ClO_4^-$ LDHs, (a.5) CoAl $CH_3COO^-$ LDHs, (a.6) CoAl $CH_3CHCOO^-$ LDHs, (a.7) CoAl $C_{12}H_{25}SO_4^-$ LDHs and (a.8) CoAl $CH_3(CH_2)_7CH{=}CH(CH_2)_7COO^-$ LDHs. (b) Photograph of a colloidal suspension of exfoliated CoAl LDH nanosheets. Reproduced with permission [56]. Copyright 2006, American Chemical Society.

precipitation method to prepare NiAl LDH/G intercalation materials with graphene (G) interspersed between LDHs host layers. The specific synthesis process is as follows, a certain amount of graphene oxide (GO) is dispersed into a mixed solution of NaOH and $Na_2CO_3$, followed by ultrasonic treatment. Then, the above dispersion was added to the mixed salt solution of $Ni(NO_3)_2$ and $Al(NO_3)_3$ and stirred vigorously at room temperature. After that, NaOH was added dropwise to adjust the pH of the solution to 10.5, and thereby the NiAl LDH/GO intercalation material was crystallized from the suspension. Finally, after reducing GO by $Na_2S$ solution, the NiAl LDH/G product was achieved. Similarly, Xu *et al.* [49] used co-precipitation method to synthesize MgAl LDH-GO, during which stripped GO was applied as substrate, $MgSO_4$ and $KAlSO_4$ solutions was added to provide metal ions, and NaOH and $Na_2CO_3$ was adopted to adjust pH to 10. The synthesizing schematic diagram is shown in Fig. 5a. The SEM image of MgAl LDH-GO in Fig. 5b shows that MgAl LDH and GO are vertically connected. The TEM image in Fig. 5c can also demonstrate the interlaced structure between nanosheets.

In brief, co-precipitation method for preparing LDHs is through the direct chemical reaction between metal ions in the solution with the precipitating agent. The preparation process is simple and the conditions are easy to control. The disadvantage is that due to the uneven local concentration of the precipitation agent during the adding process, uneven precipitation components and material agglomeration are prone to occur.

### 2.4. Anion exchange method

LDHs are composed of positively charged metal hydroxide layers and exchangeable guest anions that balance the charge between the host layers. The exchange capability of the anions in LDHs depends on the strengths of Coulomb force and hydrogen bond between the layers. A general rule is that high valence anions are easier to enter between the layers to replace low valence anions [50,51]. The types of anions are directly related to the spacings between the host layers, and can adjust the structure of LDHs [52]. On one hand, the increase of the layers' spacing can enlarge the channels for ion diffusion and storage, and increase the number of available active sites [53]. On the other hand, it can further enhance the anion exchange ability and facilitate peeling. In fact, the exchangeable guest anions are not limited to smaller inorganic ions. Some long chain organic anions can also enter the interlayer spacings and be exchanged as guests [54,55].

Liu *et al.* [56] systematically studied the process of transformation and stripping of CoAl LDHs using the anion exchange method. The primary hydrothermally synthesized CoAl $CO_3^{2-}$ LDHs are difficult to exfoliate, because the affinity between $CO_3^{2-}$ and host layers is too strong. So, it is necessary to carry out anion replacement for CoAl $CO_3^{2-}$ LDHs. Typically, CoAl $CO_3^{2-}$ LDHs are immersed in concentrated aqueous solutions of target anions. Under long term mechanical shaking, the $CO_3^{2-}$ is exchanged respectively by $Cl^-$, $NO_3^-$, $ClO_4^-$, $CH_3COO^-$, $CH_3CHCOO^-$ (lactate), $C_{12}H_{25}SO_4^-$ (dodecyl sulfate) and $CH_3(CH_2)_7CH{=}CH(CH_2)_7COO^-$ (oleate) to form LDHs with corresponding anions as the interlayer guests. The corresponding SEM images are shown in Figs. 6(a.1–a.8). By strictly controlling the pH of the solution, the crystallinity and morphology of the host layers can be kept intact in the process of anion replacement.

In the process of anion exchange, the distance between the host layers tends to increase. For example, Gonzalo and co-workers [57] converted NiFe $CO_3^{2-}$ LDH to NiFe $NO_3^-$ LDH by anion replacement, and the interlayer spacing increased from the original 7.8 Å to 7.9 Å. Liu's group vibrated and exfoliated the CoAl $NO_3^-$ LDH in formamide to obtain a stable pink colloidal solution as shown in Fig. 6b. The formamide solution is to destroy the hydrogen bonds between the host layers and allow formamide molecules to enter the interlayers of the LDHs. Under mechanical stirring or shaking conditions, LDHs peeled off into positively charged LDHs nanosheets, forming colloidal solution. The light beam was incident from the side to demonstrate the Tyndall effect, which proves that the large thick pieces of LDHs have been successfully exfoliated.

What is more, based on the exchangeability of guest species, various functional LDH-based hybrids can also be prepared [58–60]. For example, Wang *et al.* [61] inserted kojic acid, a melanin inhibitor and bacteriostatic agent, into ZnTi LDH through an anionic reaction process. The as-obtained functional ZnTi LDH has an inhibitory effect on the oxidation of bacteria and levodopa. Yan *et al.* [62] broke the traditional monotonous anion replacement method and used modifying-assembly technique to prepare bis(N-methylacridinium)@polyvinylsulfinate/LDH (BNMA@PVS/LDH) hybrid. Specifically, small BNMA divalent cations are adsorbed on the

main chains of PVS polyanions to generate BNMS@PVS ion pairs with negative charge. Then, alternate layer-by-layer assembly of negatively charged BNMS@PVS ions and positively charged LDH monolayers is carried out to obtain BNMA@PVS/LDH hybrid. This work presents a general strategy for preparing and tuning of novel LDH-based composites combining the merits of both LDH host layers and functional guest species.

All in all, anion exchange is an important method to transform and modify LDHs. In spite of the long processing period, it can realize exfoliation, modification or compositing of LDHs with other materials, which has a wide range of applications. In a word, above are the common methods for preparing LDHs with different characteristics. To endow target LDHs with more complex designs and versatile functions, combining two or more synthesizing methods is a basic strategy for future LDHs fabrication.

## 3. Applications of LDHs

### 3.1. Photo/electrocatalysis

The unique composition and structural characteristics of LDHs make it widely used in the field of photo/electrocatalysis. First of all, the bimetallic components in the host layers have multiple valence states, which can provide and accept electrons, exhibiting excellent catalytic activity. Secondly, the 2D layered structure with high specific surface area can provide or load a large number of catalytic active sites [63]. Thirdly, there is a synergistic effect between the host layers and guest layers, especially some highly conductive interlayer components, which can improve the charge transfer efficiency of LDHs and improve the photoelectric catalytic performances.

LDHs as electrocatalysts have been extensively studied in the fields of oxygen reduction reaction (ORR) [64,65], oxygen evolution reaction (OER) [66–69] and rare nitrogen reduction reaction (NRR) [70]. Yang and co-workers [71] used multi-walled carbon nanotubes (MWCNT) and rGO to prepare CoFe LDH/MWCNT/rGO intercalation composites with hierarchical porous structure. The positively charged LDHs surface is conducive to the efficient adsorption and desorption of oxygen and hydroxyl groups, and provides abundant and efficient electrocatalytic active sites for ORR and OER. MWCNT and rGO act as both carriers and electron collectors. The hierarchical porous structure allows the electrode material to have a large surface area and a large number of nanochannels, which can expose more catalytically active sites and improve the conductivity and charge transfer efficiency of the catalyst. Therefore, LDH/MWCNT/rGO shows excellent bifunctional catalytic performances for OER and ORR. Feng's group [72] used carbon fiber paper (CFP) as the conductive substrate and sodium dodecyl sulfonate (SDS) as the guest layers to grow NiFe LDHs on the CFP. The obtained NiFe SDS LDHs/CFP exhibits an overpotential of 289 mV at 10 mA/cm$^2$ for OER, which is lower than that of commercial $IrO_2$ (333 mV). This is attributed to the intercalation of SDS in NiFe LDHs, which increases the interlayer distance of LDHs from 0.76 nm to 2.49 nm, greatly increasing the specific surface area, exposing more reactive sites, and promoting the diffusion of the electrolyte.

In addition, LDHs have also been widely studied as photocatalysts [73]. For example, Lu's group [74] modified MgAl LDHs with $FeCl_3{\cdot}6H_2O$ and $FeCl_2{\cdot}4H_2O$ as iron sources, and obtained ultrathin $Fe_3O_4$/MgAl LDHs as an effective photocatalyst for reducing carbon dioxide. Among them, $Fe_3O_4$ can promote the transfer of electron-hole pairs in the photocatalyst and improve the separation efficiency of charge carriers. The 2D structure of MgAl LDHs can effectively reduce the transmission resistance of carriers, and meanwhile create more active sites and improve photocatalytic efficiency. In addition, the magnetism of $Fe_3O_4$ facilitates the recycling process of the catalyst [75]. $CO_2$ is the main factor that causes the greenhouse effect, and reasonable modification of LDHs materials can achieve good photocatalytic activity to reduce $CO_2$. Zhao *et al.* [76] found that ultra-thin ZnAl-LDH nanosheets containing a large number of oxygen deficiencies can effectively absorb $CO_2$, and the oxygen vacancies can improve light-induced charge separation, which is the adsorption site of $CO_2$. At present, LDHs photocatalysts can reduce $CO_2$ to CO [14], methanol [77], hydrogen and methane [78,79]. The Zn-containing system can effectively increase the conversion rate of $CO_2$ to CO, and the Cu-containing LDHs can effectively convert $CO_2$ to methanol.

### 3.2. Electrochemical energy storage

As important energy storage devices, supercapacitor and battery have become research hotspots in new energy fields [80–85]. The divalent and trivalent LDHs, with high redox activity and 2D layered structures, exhibit abundant electrochemical active sites and efficient charge/mass transport routes. Benefiting from the highly accessible active surface area and good mechanical stability, LDHs can provide high theoretical specific capacity and good cycle stability, which is suitable to be applied as electrode materials for supercapacitors [86–88] and batteries [89,90].

Compared with traditional batteries and dielectric capacitors, supercapacitors have the advantages of high power density, long cycle life, low maintenance costs, environmental friendliness and high safety, making it a promising type of electrochemical energy storage device [91–93]. In recent years, the application of LDHs materials to the research and development in supercapacitor electrode materials are in the ascendant [94,95]. Feng's group [96] prepared and regulated $Ni_{1-x}Co_x$ $SO_4^{2-}$ LDHs by controlling the molar ratio of $Ni^{2+}$ and $Co^{2+}$, and studied the effect of "1-x: x" on the morphology and energy storage performance of the material. As shown in Fig. 7a, as the $Co^{2+}$ content increases, the current peak values of the cyclic voltammograms (CV) firstly rise and then fall. When the value of "x" was 0.65, $Ni_{0.35}Co_{0.65}$ $SO_4^{2-}$ LDHs had the largest current peak value. Similarly, in the constant current charge and discharge test (GCD) shown in Fig. 7b, $Ni_{0.35}Co_{0.65}$ $SO_4^{2-}$ LDHs displayed the longest discharge time. It can be concluded that when the molar ratio of Ni to Co is 0.35:0.65, the supercapacitor electrode had the highest specific capacitance. The main reason is that the interlayer spacing of $Ni_{0.35}Co_{0.65}$ $SO_4^{2-}$ LDHs increased first and then decreased with the increase of Co content. When the value of "x" is 0.65, the interlayer spacing can reach as wide as 9.05 Å, and the self-aggregation tendency of nanosheets is the smallest. At the same time, the flaky structure of LDHs has obvious folds, which can provide abundant reaction sites and ion diffusion channels. Zhang and co-workers [97] chose surfactant sodium oleate as the intercalation agent, which could increase the interlayer spacing of LDHs to 43.7 Å. The as obtained NiAl LDH/sodium oleate nanosheet intercalation material shows an extremely high layer spacing, which effectively shortened the electron/ion diffusion distance and increased the storage capacity of ions in the interlayer channel. A high specific capacitance of 1.040 C/cm$^2$ at a current density of 1.68 mA/cm$^2$ was achieved for NiAl LDH/sodium oleate based electrode. After 2000 cycles, it still maintained 88.25% of the initial capacitance, demonstrating its application potential as an electrode material for supercapacitors with high stability.

Taking the low conductivity of LDHs into account, most researchers combine them with highly conductive carbon materials to further improve their performance as electrode materials. For example, Gao's group [98] used GO as substrate to uniformly grow NiAl LDHs on its surface by hydrothermal method to obtain GO/NiAl LDHs composite material. GO can separate adjacent LDHs flakes, and effectively increase the specific surface area. The electrode made of this material has excellent cycle stability. Af-

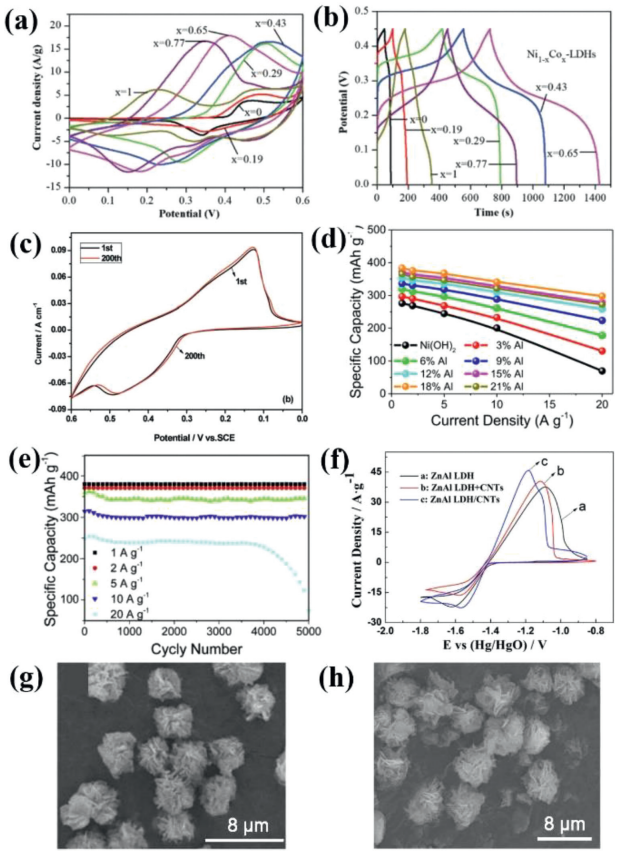


**Fig. 7.** (a) CV curves of $Ni_{1-x}Co_x$ LDHs in 2 mol/L KOH. (b) GCD curves at a current density of 1 A/g. Reproduced with permission [96], Copyright 2020, American Scientific Publishers. (c) CV curves of the GO/NiAl LDHs composite at the 1st and 200th cycles. (d) Specific capacitance of the LDHs electrodes containing various Al contents at different current densities. Reproduced with permission [98]. Copyright 2011, American Chemical Society. (e) Cycling life curves of NiAl LDHs (18% Al) at different charge-discharge rates. Reproduced with permission [100]. Copyright 2018, Elsevier. (f) CV curves for zinc electrodes with ZnAl LDH, ZnAl LDH/CNTs and ZnAl LDH/CNTs. SEM images of ZnAl LDH/CNTs (g) before and (h) after testing. Reproduced with permission [101]. Copyright 2018, Elsevier.

ter 50 cycles of testing, it reaches the highest specific capacitance (781.5 F/g), which is an increase of 38.07% from the initial value. As shown in Fig. 7c, after 200 cycles, the current value was basically unchanged, indicating that the composite material had good electrochemical reversibility. Zou's group [99] alternately assembled G and layered NiAl LDH to obtain G/NiAl LDH material. NiAl LDH prevented the re-stacking of G, and G improved the conductivity of the material. The synergy between the G and LDH made the G/NiAl LDH exhibit excellent electrochemical performance and can be used as an electrode material for supercapacitors.

In addition, LDHs also have some applications in batteries. For instance, Pan *et al.* [100] used NiAl LDHs as the cathode material for nickel-metal hydride (Ni/MH) secondary batteries. As shown in Fig. 7d, when the amount of Al is 18% of the total metal content, the highest specific capacity of 383.4 mAh/g was exhibited at a current density of 1 A/g. Also, as shown by the long cycle curves of NiAl LDHs (with 18% Al) under different discharging current densities in Fig. 7e, the material also showed good stability. Liu's group [101] synthesized ZnAl LDH/CNTs with CNTs as conductive substrate, which was used as anode material of zinc-nickel secondary batteries. The highly connected conductive network composed of CNTs and abundant LDHs nanosheets made the CV curves of ZnAl LDH/CNTs have the largest redox peak, as shown in Fig. 7f. It can be seen from the SEM images in Figs. 7g and h that the flower-like morphology of ZnAl LDH/CNTs remains unchanged before and after 300 charge-discharge cycles, indicating that the material not only has high specific capacity but also has excellent cycle stability.

### 3.3. Magnetic materials

The movement of electrons inside the material is the fundamental reason for magnetism. Negatively charged electrons move around the nucleus at high speeds to produce a magnetic moment. Magnetic moment is a physical quantity that characterizes the strength of magnetism, and its size depends on the electronic structure of the material itself. The electron arrangement in atoms follows the Pauli incompatibility and lowest energy principle. For example, the 3d orbitals of transition metals (Fe, Co, Ni) are not fulfilled with extranuclear electrons, and the spin magnetic moments of the electrons cannot cancel each other, which is the direct reason why these atoms exhibit magnetism [102–104]. The structure of LDHs itself is quite special. Specifically, each regular octahedral structure has six $M^{2+}/M^{3+}$-O units. Studies have shown that $M^{2+}$-O-$M^{2+}$, $M^{3+}$-O-$M^{2+}$ and $M^{3+}$-O-$M^{3+}$ exhibit ferromagnetism or antiferromagnetic properties. In addition, when guest components are introduced between the LDHs host layers, the magnetic properties will also be changed due to the altered electronic structure caused by intercalation. Thereby, some LDHs intercalation materials can be tuned to exhibit spontaneous magnetization, ferromagnetism or ferrimagnetism [105–107].

The layer spacing, metal ratio and morphology of LDHs will all affect the magnetic properties of the material. Leroux's group [108] adjusted the layer spacing of $Co_2Al$ LDHs from 7.6 Å to 25 Å by using surfactant molecules. The increase of the layer spacing caused the change of the dipole moment between the layers, and finally caused the magnetic change of the material. The effect of the spacing between the layers on the magnetic induction behavior also proves that there is a weak interaction between the layers. Almansa and co-workers [109] synthesized $Ni_xCr$ $CO_3^{2-}$ LDHs with different metal ratios by changing the metal ratio in the solution, and the ratios of $Ni^{2+}$-O-$Ni^{2+}$, $Cr^{3+}$-O-$Ni^{2+}$ and $Cr^{3+}$-O-$Cr^{3+}$ in the material were different. Among them, $Ni^{2+}$-O-$Ni^{2+}$ shows ferromagnetism, and $Cr^{3+}$-O-$Ni^{2+}$ and $Cr^{3+}$-O-$Cr^{3+}$ show antiferromagnetic properties. The final magnetic properties of the material are the result of the competition between ferromagnetism and antiferromagnetic components. Under high temperature paramagnetic conditions, the higher the $Cr^{3+}$ content, the higher the contents of the antiferromagnetic $Cr^{3+}$-O-$Ni^{2+}$ and $Cr^{3+}$-O-$Cr^{3+}$ pairs. Coronado *et al.* [110] inserted copper(II) phthalocyaninetetrasulfonate complexes (CuPcTs) between the host layers of LDHs by anion exchange method, and took advantage of the different interactions between CuPcTs and the host layers to prepare materials with different magnetic properties, such as diamagnetic ZnAl LDHs and ferromagnetic NiAl LDHs. In addition, the morphology also affects the magnetic properties of LDHs materials. For example, Abellán *et al.* [111] prepared hexagonal CoAl LDH and flower-like NiFe LDH as shown in Fig. 8a. Compared with the hexagonal flakes, the flower-like LDH has a certain curvature for the petals. The deformation of the nanoflakes would cause dislocation of the crystals and lead to more disordered magnetic behaviors for flower-like LDH, which shows stronger antiferromagnetism depicted in Fig. 8b.

Magnetic materials have been involved in many aspects of production and daily life, from cutting-edge technology to industrial automation and household appliances. It is of high value to use the adjustability of the structure and composition of LDHs to achieve the design and regulation of magnetic properties of materials.

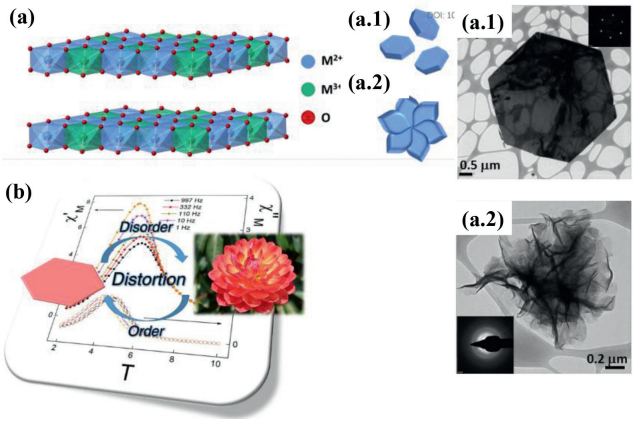


**Fig. 8.** (a) Schematic diagram of LDH with a $M^{2+}/M^{3+}$ ratio of 2:1: Schematic structure and TEM images of (a.1) hexagonal CoAl LDH and (a.2) flower-shaped CoAl LDH. (b) Magnetic behaviors of CoAl LDH with different morphologies. Reproduced with permission [111]. Copyright 2018, Royal Society of Chemistry.

### 3.4. Pollutant adsorption

Excessive emission of toxic substances into the natural world is bound to pose a threat to the ecosystem and human health [112]. The inherent 2D structural characteristics of LDHs, such as large specific surface area, exchangeability of anions and flexible interlayer space make it a promising pollutant adsorption material. In addition to electrostatic adsorption, the adsorption process also relates to the hydrogen bonds formed between $OH^-$ in LDHs and functional groups in pollutants [113,114] .

Li *et al.* [115] used polyethylene glycol to prepare carbon dots material with a large amount of oxygen-containing functional groups, and then assembled positively charged MgAl LDHs with carbon dots to prepare a lightweight and environmentally friendly LDH-carbon dots composite for the adsorption of methyl blue dye, as shown in Fig. 9a. The adsorption behaviors of materials in 80 mg/L methyl blue aqueous solution are shown in Fig. 9b. It can be seen that under the same adsorption conditions, the adsorption rate of methyl blue on LDH-carbon dots composite is as high as 96%, while pure LDH can only adsorb 45%. This is because, aside from the strong electrostatic adsorption between LDH and methyl blue, the attachment of carbon dots on the surface of LDH can promote the formation of hydrogen bonds between the composite material and methyl blue. Combining the advantages of LDH and carbon dots, the adsorption capability of the composite for anionic methyl blue dye is as high as 185 mg/g, as demonstrated by Fig. 9c. The inset in Fig. 9c is a photograph of the LDH-carbon dots composite before and after the adsorption of methyl blue. It is obvious that the powder turns black after dye adsorption. Al-Ghamdi *et al.* [116] grows NiFe LDHs nanosheets on carbon fiber (CF), and the obtained CF/NiFe LDHs can be used to remove methyl orange (MO) and Congo red (CR) anionic dyes. Its adsorption performance is much better than pure CF and NiFe LDHs, and CF/NiFe LDHs has the advantages of recyclability and more stability.

Ma *et al.* [117] inserted polysulfide ($S_x^{2-}$, $x=2,4$) into MgAl LDHs, and the formed $S_x^{2-}$ LDH composite material exhibited rapid capture and good selection of uranium ($UO_2^{2+}$), a type of radioactive pollutant, in various aqueous solutions. Its adsorption coefficient ($K_d^u = 3.4 \times 10^6$ mL/g) is the maximum reported so far. The adsorption mechanism is schematically presented in Fig. 9d. Obviously, LDHs mainly relies on surface adsorption and interlayer anion exchange to remove or fix radioactive $UO_2^{2+}$. When the $UO_2^{2+}$ concentration is low, $S_4^{2-}$ and $UO_2^{2+}$ form a complex and remain in the host of LDH. When the concentration of $UO_2^{2+}$ is high, $S_4^{2-}$ and $UO_2^{2+}$ form a neutral salt $UO_2S_4$, and other anions in the water such as $NO_3^-$ and $Cl^-$ will enter LDH to form $NO_3^-$ LDH and $Cl^-$ LDH. This process is mainly affected by the nature of the charge balance anion in the interlayer space, the layer charge density and the distance between the layers. In addition to the above description, LDHs materials have also been studied in heavy metal removal [118,119] and oil adsorption [120,121].

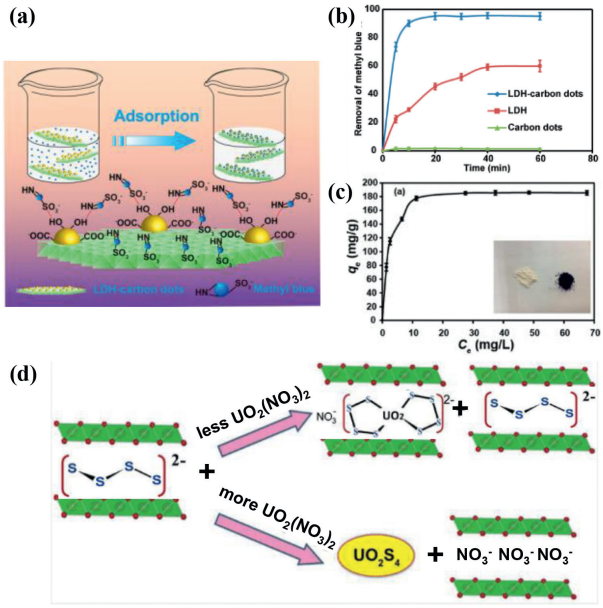


**Fig. 9.** (a) Schematic diagram of the active sites for methyl blue adsorption on the LDH-carbon dot composite. (b) Adsorption percentages of methyl blue on carbon dots, LDH and LDH-carbon dots. (c) Methyl blue adsorption line of LDH-carbon dots composite. Reproduced with permission [115]. Copyright 2014, American Chemical Society. (d) Schematic diagram of the mechanism of $S_x^{2-}$ LDH material adsorbing $UO_2^{2+}$. Reproduced with permission [117]. Copyright 2015, American Chemical Society.

### 3.5. Other applications

In addition to the various applications described above, the particularity of the LDHs structure and the synergy between the intercalation layers make it show potential applications in many other fields. For example, in order to solve the problem of incompatibility between gas barrier and ion conduction in membrane materials, Han and co-workers [122] assembled LDH nanosheets and quaternary ammonium modified polysulfone (QAPSF) layer by layer, which is schematically shown in Fig. 10a. The $(LDH/QAPSF)_n$ material combines the ionic conductivity of LDH and the gas barrier properties of QAPSF, making it suitable as fuel cell ion exchange membranes that requires both ion conduction and gas barrier. From the molecular structure and $^1H$ NMR spectrum of QAPSF in Figs. 10b and c, it can be seen that QAPSF has a large molecular structure, which can effectively prevent the overlap of LDHs layers. In addition, using LDHs as the host and sunscreen molecules as the guest, the assembled sunscreen/LDHs composite materials can prevent the sunscreen molecules from directly contacting human skin, reduce the residue of toxic substances, and protect the skin [123]. P-aminobenzoic acid (PABA) and cinnamic acid are effective ingredient in sunscreens. Li *et al.* [124] inserted PABA as guest into LDHs to form a PABA/LDHs composite material that can reduce the production of free radicals ($OH^-$ and $O_2^-$) and slow down skin aging. Wang *et al.* [125] inserted cinnamic acid into ZnTi LDH sheets by anion exchange method. The synergistic effect of cinnamic acid and LDH can improve the absorption capability of ultraviolet rays.

What is more, the special interaction between the host and guest layers, the adjustable crystalline size, the high loading ca-

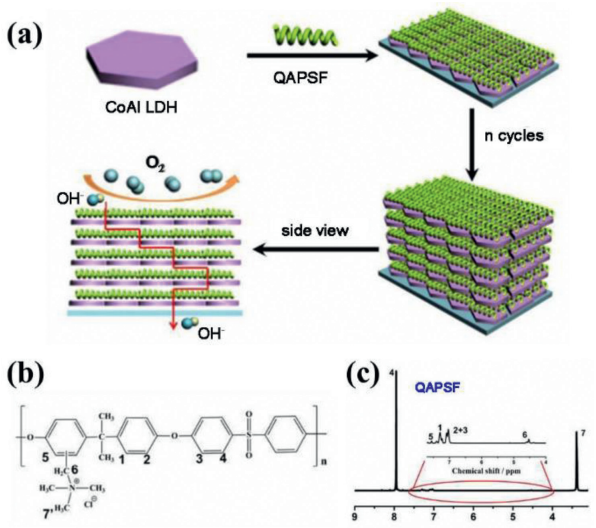


**Fig. 10.** (a) Schematic illustration for the assembly process of $(LDH/QAPSF)_n$ films with gas barrier and ion conductive properties. (b) Chemical structure of QAPSF. (c) $^1H$ NMR spectrum of QAPSF. Reproduced with permission [122]. Copyright 2018, American Chemical Society.

pability of different molecules/species and the biocompatibility of LDHs have also made certain progress in medical, security and other multifunctional applications, such as bio-imaging techniques [126,127], early disease diagnosis [128–130], drug delivery [131–133], sensor and anti-counterfeiting systems [134–137].

## 4. Summary and prospect

In summary, the preparation, structure and composition control of LDHs can be achieved through hydrothermal, electrodeposition, co-precipitation, anion exchange and other methods, thereby meeting the application needs of different fields such as catalysis, electrochemical energy storage, magnetic materials, pollutant adsorption and so on. More importantly, the unique layered stacked structure of LDHs can achieve intercalation and compounding with different functional components to purposely improve different performances. As a way of outlook, the study and application of LDHs will continuously make progress and face challenges. The critical issues and prospects of LDH-based materials in future development may lie in the following two aspects:

(i) From the perspective of preparation, although the synthesizing processes for individual LDHs are mature and easy to realize large-scale production, the methods for constructing LDH-based intercalation materials are still limited and mainly based on stripping-assembly techniques. The current technology for stripping LDHs still has the defects of tediousness, low yield and poor controllability, which greatly inhibits the large-scale and high-quality preparation of stripped LDH monolayers. For the following intercalation process, LDH host layers and guest species are mainly assembled through electrostatic forces and hydrogen bonding, which are relatively weak and easy to fall off after long-term usage. Therefore, for the sake of easy-preparation and performance-stability in practical applications, it is highly required to explore the fundamental factors that affect the intercalation structure and develop in-situ synthesizing strategies for more efficient and firm construction of LDH-based hybrid materials.

(ii) From the perspective of application, although significant progress has been made for applying LDH-based nanomaterials in various fields, the basic principles and mechanisms on performance regulation are not clear enough. Hence, in future studies, experimental characterization and theoretical calculations can be combined to discuss in depth the relationship between the 2D confinement effects and material properties, and provide theoretical guidance for compositional/structural design, assembly and performance optimization of LDH-based materials. This is also of great significance for rational design and construction of new LDHs with target structures and functions, in order to solve specific problems in real industry.

## Declaration of competing interest

The authors declare no conflict of interest.

## Acknowledgments

This work was financially supported by National Natural Science Foundation of China (No. 52102100), Industry-University-Research Cooperation Project of Jiangsu Province (No. BY2021525), and Key Research and Development Program (Social Development) of Zhenjiang City (No. SH2019009).

## References

[1] X. Zou, A. Goswami, T. Asefa, J. Am. Chem. Soc. 135 (2013) 17242–17245.
[2] X. Wang, H. Yan, J. Zhang, et al., J. Alloys Compd. 810 (2019) 151911.
[3] P. Li, Q. Xie, L. Zheng, et al., Nano Res. 10 (2017) 2988–2997.
[4] L. Li, W. Gu, J. Liu, et al., Nano Res. 8 (2014) 682–694.
[5] X. Zhao, C. Niu, L. Zhang, et al., Chemosphere 204 (2018) 11–21.
[6] Y. Wang, X. Liu, N. Zhang, et al., Appl. Clay Sci. 165 (2018) 277–283.
[7] Y. Yang, J. Wu, T. Xiao, et al., Appl. Catal. B: Environ. 255 (2019) 117771.
[8] D. Zhong, T. Li, D. Wang, et al., Nano Res. 15 (2022) 162–169.
[9] T. Wang, X. Liu, Y. Li, et al., Nano Res. 13 (2019) 79–85.
[10] H. Zhang, F. Huang, D.L. Liu, P. Shi, Chin. Chem. Lett. 26 (2015) 1137–1143.
[11] Y. Li, R. Zhang, J. Li, et al., Chin. Chem. Lett. 32 (2021) 1165–1168.
[12] M. Duan, M. Qiu, S. Sun, et al., Appl. Clay Sci. 216 (2022) 106360–106367.
[13] S. Naseem, B. Gevers, R. Boldt, et al., RSC Adv. 9 (2019) 3030–3040.
[14] K.I. Katsumata, K. Sakai, K. Ikeda, et al., Mater. Lett. 107 (2013) 138–140.
[15] B. Du, Z. Fang, Nanotechnology 21 (2010) 315603–315608.
[16] M.V. Bukhtiyarova, J. Solid State Chem. 269 (2019) 494–506.
[17] M. Shao, R. Zhang, Z. Li, et al., Chem. Commun. 51 (2015) 15880–15893.
[18] H. Liu, X. Zhao, Y. Zhu, H. Yan, Phys. Chem. Chem. Phys. 22 (2020) 2521–2529.
[19] M. Zhao, Q. Zhang, J. Huang, F. Wei, Adv. Funct. Mater. 22 (2012) 675–694.
[20] J. Leng, P.J. Purohit, N. Kang, et al., Eur. Polym. J. 68 (2015) 338–354.
[21] X. Wang, J. Zhang, S. Yang, et al., Electrochim. Acta 295 (2019) 1–6.
[22] Y. Jiang, Z. Yang, L. Liu, et al., Mater. Lett. 255 (2019) 126558.
[23] W. Liang, H. Yan, X. Feng, et al., Appl. Catal. A: Gen. 597 (2020) 117551.
[24] J. Zhu, Z. Zhu, H. Zhang, et al., RSC Adv. 9 (2019) 2284–2291.
[25] R. Li, Y. Wang, W. Li, et al., Chem. Commun. 55 (2019) 13370–13373.
[26] F. Song, X. Hu, Nat. Commun. 5 (2014) 4477.
[27] H. Liu, T. Yu, D. Su, et al., Ceram. Int. 43 (2017) 14395–14400.
[28] Y. Xiao, D. Su, X. Wang, et al., Electrochim. Acta 253 (2017) 324–332.
[29] Y. Lu, B. Jiang, L. Fang, et al., J. Alloys Compd. 714 (2017) 63–70.
[30] Z. Cai, D. Zhou, M. Wang, et al., Angew. Chem. Int. Ed. 57 (2018) 9392–9396.
[31] M.B. Stevens, C.D.M. Trang, L.J. Enman, et al., J. Am. Chem. Soc. 139 (2017) 11361–11364.
[32] M. Jiang, X. Zhang, J. Alloys Compd. 794 (2019) 13–20.
[33] C.W. Jeon, S.S. Lee, I.K. Park, Appl. Surf. Sci. 473 (2019) 65–69.
[34] T. Wen, X. Wu, X. Tan, et al., ACS Appl. Mater. Interfaces 5 (2013) 3304–3311.
[35] Y. Pei, Y. Yang, F. Zhang, et al., ACS Appl. Mater. Interfaces 9 (2017) 31887–31896.
[36] N. Jiang, B. You, M. Sheng, Y. Sun, Angew. Chem. Int. Ed. 54 (2015) 6349–6352.
[37] X. Xu, P. Du, Z. Chen, M. Huang, J. Mater. Chem. A 4 (2016) 10933–10939.
[38] X. Yu, M. Zhang, W. Yuan, G. Shi, J. Mater. Chem. A 3 (2015) 6921–6928.
[39] R. Yang, Y. Zhou, Y. Xing, et al., Appl. Catal. B 253 (2019) 131–139.
[40] F. Dionigi, P. Strasser, Adv. Energy Mater. 6 (2016) 1600621.
[41] J. Shi, N. Du, W. Zheng, et al., Chem. Eng. J. 327 (2017) 9–17.
[42] X.R. Wang, Y. Li, L.P. Tang, et al., Chin. Chem. Lett. 28 (2017) 394–399.
[43] H. Xu, J. Wu, J. Liu, et al., J. Mater. Sci. Mater. Electron. 29 (2018) 17234–17244.
[44] A. Smalenskaite, D.E.L. Vieira, A.N. Salak, et al., Appl. Clay Sci. 143 (2017) 175–183.
[45] Y. Huang, T. Yang, M. Liang, et al., Chemosphere 235 (2019) 143–152.
[46] B.M. Hunter, W. Hieringer, J.R. Winkler, et al., Energy Environ. Sci. 9 (2016) 1734–1743.
[47] Y. Xu, Y. Hao, G. Zhang, et al., RSC Adv. 5 (2015) 55131–55135.
[48] M. Li, J.E. Zhu, L. Zhang, et al., Nanoscale 3 (2011) 4240–4246.
[49] Y. Gao, Z. Wei, J. Xu, Electrochim. Acta 330 (2020) 135195.
[50] L. Dang, H. Liang, J. Zhuo, et al., Chem. Mater. 30 (2018) 4321–4330.
[51] D. Zhou, Z. Cai, Y. Bi, et al., Nano Res. 11 (2018) 1358–1368.
[52] H. Liang, F. Meng, M. Cabán-Acevedo, et al., Nano Lett. 15 (2015) 1421–1427.
[53] M. Zhou, L. Yan, H. Ling, et al., Appl. Surf. Sci. 404 (2017) 246–253.

[54] M. Wang, Y. Li, J. Ji, et al., Chin. Chem. Lett. 24 (2013) 593–596.
[55] S.R. Tavares, J.F.S. Haddad, P.I.R. Moraes, A.A. Leitão, Appl. Surf. Sci. 513 (2020) 145743.
[56] Z. Liu, R. Ma, M. Osada, et al., J. Am. Chem. Soc. 128 (2006) 4872–4880.
[57] G. Abellán, E. Coronado, C. Martí-Gastaldo, et al., J. Mater. Chem. 20 (2010) 7451–7455.
[58] Q. Wang, D. O'hare, Chem. Rev. 112 (2012) 4124–4155.
[59] R. Gao, D. Yan, X. Duan, Cell Rep. Phys. Sci. 2 (2021) 100536.
[60] R. Gao, J. Zhu, D. Yan, Nanoscale 13 (2021) 13593–13603.
[61] X.R. Wang, H.M. Cheng, X.W. Gao, et al., Chin. Chem. Lett. 30 (2019) 919–923.
[62] D. Yan, J. Lu, L. Chen, et al., Chem. Commun. 46 (2010) 5912–5914.
[63] R. Gao, D. Yan, Adv. Energy Mater. 10 (2020) 1900954.
[64] M. Zhang, J. Zhang, S. Ran, et al., Nano Res. 14 (2020) 1175–1186.
[65] S.A. Chala, M.C. Tsai, W.N. Su, et al., ACS Catal. 9 (2019) 117–129.
[66] R. Gao, D. Yan, Nano Res. 11 (2018) 1883–1894.
[67] Z. Lu, L. Qian, W. Xu, et al., Nano Res. 9 (2016) 3152–3161.
[68] Z. Zhao, Q. Shao, J. Xue, et al., Nano Res. 15 (2022) 310–316.
[69] R.C. Rohit, A.D. Jagadale, S.K. Shinde, et al., J. Alloys Compd. 863 (2021) 158081.
[70] M. Arif, G. Yasin, L. Luo, et al., Appl. Catal. B: Environ. 265 (2020) 118559.
[71] Y.J. Yang, M. Duan, C. Yan, et al., J. Electroanal. Chem. 856 (2020) 113697.
[72] H. Zhong, X. Cheng, H. Xu, et al., Electrochim. Acta 258 (2017) 554–560.
[73] L. Yao, D. Wei, D. Yan, C. Hu, Chem. Asian J. 10 (2015) 630–636.
[74] N. Gao, Z. Lu, X. Zhao, et al., Chem. Eng. J. 304 (2016) 351–361.
[75] G. Gao, Z. Zhu, J. Zheng, et al., J. Colloid Interf. Sci. 555 (2019) 1–10.
[76] Y. Zhao, G. Chen, T. Bian, et al., Adv. Mater. 27 (2015) 7824–7831.
[77] M.M.J. Li, C. Chen, T. Ayvalı, et al., ACS Catal. 8 (2018) 4390–4401.
[78] K. Świrk, M. Motak, T. Grzybek, et al., React. Kinet. Inet. Mech. Cat. 126 (2019) 611–628.
[79] C. Sun, K. Świrk, D. Wierzbicki, et al., Int. J. Hydrog. Energy 46 (2021) 12169–12179.
[80] P. Wang, B. Xi, M. Huang, et al., Adv. Energy Mater. 11 (2021) 2002893.
[81] X. Wang, Z. Zhang, B. Xi, et al., ACS Nano 15 (2021) 9244–9272.
[82] M. Huang, B. Xi, N. Shi, et al., Small Struct. 2 (2021) 2000085.
[83] J. Chen, X. Guo, M. Gao, et al., Chem. Commun. 57 (2021) 10580–10583.
[84] D. Su, M. Huang, J. Zhang, et al., Nano Res. 13 (2020) 2862–2868.
[85] X. Guo, W. Zhang, J. Shi, et al., Nano Res. 15 (2022) 2092–2103.
[86] Q. Sun, K. Yao, Y. Zhang, Chin. Chem. Lett. 31 (2020) 2343–2346.
[87] N.L.W. Septiani, Y.V. Kaneti, K.B. Fathoni, et al., Nano Energy 67 (2020) 104270.
[88] H. Gao, Y. Cao, Y. Chen, et al., Appl. Surf. Sci. 465 (2019) 929–936.
[89] E. Shangguan, H. Zhang, C. Wu, et al., Electrochim. Acta 330 (2020) 135198.
[90] J. He, W. Zhou, D. Zhu, et al., ACS Sustain. Chem. Eng. 8 (2020) 14877–14885.
[91] R. Patel, J.T. Park, M. Patel, et al., J. Mater. Chem. A 6 (2018) 12–29.
[92] J. Li, P. Zhang, X. Zhao, et al., J. Colloid Interf. Sci. 549 (2019) 236–245.
[93] D. Zhang, X. Guo, X. Tong, et al., J. Alloys Compd. 837 (2020) 155529.
[94] G. Wang, Z. Jin, W. Zhang, J. Colloid Interf. Sci. 577 (2020) 115–126.
[95] D. Wei, Y. Zhang, X. Zhu, et al., J. Alloys Compd. 824 (2020) 153937.
[96] Y. Feng, Y. Li, W. Yang, H. Huang, J. Nanosci. Nanotechnol. 20 (2020) 1260–1268.
[97] H. Zhang, M. Usman Tahir, X. Yan, et al., Chem. Eng. J. 368 (2019) 905–913.
[98] Z. Gao, J. Wang, Z. Li, et al., Chem. Mater. 23 (2011) 3509–3516.
[99] Y. Wimalasiri, R. Fan, X.S. Zhao, L. Zou, Electrochim. Acta 134 (2014) 127–135.
[100] Y. Nie, W. Li, J. Pan, et al., Electrochim. Acta 289 (2018) 333–341.
[101] L. Liu, M. Cheng, Z. Yang, Electrochim. Acta 277 (2018) 67–76.
[102] T. Suetsuna, H. Kinouchi, T. Kawamoto, N. Sanada, J. Magn. Magn. Mater. 473 (2019) 416–421.
[103] Y. Sun, X. Zhou, Y. Liu, et al., Mater. Res. Bull. 45 (2010) 878–881.
[104] E. Howard, Contemp. Phys. 60 (2019) 339–340.
[105] K.F. Mak, J. Shan, D.C. Ralph, Nat. Rev. Phys. 1 (2019) 646–661.
[106] R.Y. Babkin, Y.G. Pashkevich, A.V. Fedorchenko, et al., J. Magn. Magn. Mater. 473 (2019) 501–504.
[107] T. Sheng, Z. Zhang, Y. Hu, et al., Environ. Sci. Pollut. Res. 26 (2019) 7102–7114.
[108] M. Intissar, R. Segni, C. Payen, et al., J. Solid State Chem. 167 (2002) 508–516.
[109] J.J. Almansa, E. Coronado, C. Martí-Gastaldo, A. Ribera, Eur. J. Inorg. Chem. 2008 (2008) 5642–5648.
[110] G. Abellán, F. Busolo, E. Coronado, et al., J. Phys. Chem. C 116 (2012) 15756–15764.
[111] J.A. Carrasco, G. Abellán, E. Coronado, J. Mater. Chem. C 6 (2018) 1187–1198.
[112] K. Ariga, J.A. Jackman, N.J. Cho, et al., Chem. Rec. 19 (2019) 1891–1912.
[113] L. Lupa, L. Cocheci, R. Pode, I. Hulka, Sep. Purif. Technol. 196 (2018) 82–95.
[114] C. Zhang, S. Yang, H. Chen, et al., Appl. Surf. Sci. 301 (2014) 329–337.
[115] M. Zhang, Q. Yao, C. Lu, et al., ACS Appl. Mater. Interfaces 6 (2014) 20225–20233.
[116] H. Hu, S. Wageh, A.A. Al-Ghamdi, et al., Appl. Surf. Sci. 511 (2020) 145570.
[117] S. Ma, L. Huang, L. Ma, et al., J. Am. Chem. Soc. 137 (2015) 3670–3677.
[118] L. Ma, Q. Wang, S.M. Islam, et al., J. Am. Chem. Soc. 138 (2016) 2858–2866.
[119] L. Ma, S.M. Islam, C. Xiao, et al., J. Am. Chem. Soc. 139 (2017) 12745–12757.
[120] X. Yue, J. Li, T. Zhang, et al., Chem. Eng. J. 328 (2017) 117–123.
[121] S.S. Elanchezhiyan, S. Meenakshi, Int. J. Biol. Macromol. 104 (2017) 1586–1595.
[122] X. Xu, L. Wang, J. Wang, et al., Chem. Commun. 54 (2018) 7778–7781.
[123] T.a.D. Silva, T.a.D. Silva, T.G.D. Nascimento, et al., Einstein (Sao Paulo) 17 (2019) eRW4456.
[124] Y. Li, L. Tang, W. Zhou, X. Wang, Chin. Chem. Lett. 27 (2016) 1495–1499.
[125] Y. Li, L. Tang, X. Ma, et al., J. Phys. Chem. Solids 107 (2017) 62–67.
[126] Y. Weng, S. Guan, H. Lu, et al., Talanta 184 (2018) 50–57.
[127] H. Zuo, W. Chen, B. Li, et al., Chem. Eur. J. 23 (2017) 14299–14306.
[128] G. Carja, E.F. Grosu, C. Petrarean, N. Nichita, Nano Res. 8 (2015) 3512–3523.
[129] W. Xie, Z. Guo, Z. Cao, et al., ACS Biomater. Sci. Eng. 5 (2019) 2555–2562.
[130] W. Chen, H. Zuo, E. Zhang, et al., ACS Appl. Mater. Interfaces 10 (2018) 20326–20333.
[131] X. Mei, S. Xu, T. Hu, et al., Nano Res. 11 (2017) 195–205.
[132] W. Chen, J. Ouyang, H. Liu, et al., Adv. Mater. 29 (2017) 1603864.
[133] Y.J. Son, I.C. Lee, H.H. Jo, et al., J. Korean Ceram. Soc 56 (2019) 56–64.
[134] R. Gao, M.S. Kodaimati, D. Yan, Chem. Soc. Rev. 50 (2021) 5564–5589.
[135] H. Ma, R. Gao, D. Yan, et al., J. Mater. Chem. C 1 (2013) 4128–4137.
[136] R. Gao, D. Yan, D.G. Evans, X. Duan, Nano Res. 10 (2017) 3606–3617.
[137] B. Hai, Y. Zou, G. Guo, et al., Chin. Chem. Lett. 28 (2017) 149–152.